JACS
JOURNAL OF THE AMERICAN CHEMICAL SOCIETY

Article

pubs.acs.org/JACS

Hierarchical Self-Assembly of Discrete Organoplatinum(II) Metallacycles with Polysaccharide via Electrostatic Interactions and Their Application for Heparin Detection

Li-Jun Chen,[†] Yuan-Yuan Ren,[†] Nai-Wei Wu,[†] Bin Sun,[†,‡] Jian-Qiu Ma,[⊥] Li Zhang,[∥] Hongwei Tan,[⊥] Minghua Liu,[∥] Xiaopeng Li,[‡] and Hai-Bo Yang*[,†]

[†]Shanghai Key Laboratory of Green Chemistry and Chemical Processes, Department of Chemistry, East China Normal University, Shanghai 200062, PR China

[‡]Department of Chemistry and Biochemistry & Materials Science, Engineering, and Commercialization Program, Texas State University, San Marcos, Texas 78666, United States

[∥]Key Laboratory of Colloid, Interface and Chemical Thermodynamics, Institute of Chemistry, The Chinese Academy of Sciences, Beijing, 100080, PR China

[⊥]Department of Chemistry, Beijing Normal University, Beijing 100050, PR China

Supporting Information

ABSTRACT: In recent past years, investigation of hierarchical self-assembly for constructing artificial functional materials has attracted considerable attention. Discrete metallacycles based on coordination bonds have proven to be valid scaffolds to fabricate various supramolecular polymers or smart soft matter through hierarchical self-assembly. Here, we present the first example of the hierarchical self-assembly of discrete metallacycles by taking advantage of the positive charges of the organoplatinum(II) metallacycle skeleton through multiple electrostatic interactions. Heparin, a sulfated glycosaminoglycan polymer that has been widely used as an anticoagulant drug, was selected to induce hierarchical self-assembly because of the existence of multiple negative charges. To investigate the hierarchical self-assembly process, an aggregation-induced emission (AIE) active moiety, tetra-phenylethylene (TPE), was introduced onto the metallacycle via coordination-driven self-assembly. Photophysical studies revealed that the addition of heparin to the tris-TPE metallacycles solution resulted in dramatic fluorescence enhancement, which supported the aggregation between metallacycle and heparin driven by multiple electrostatic interactions. Moreover, the entangled pearl-necklace networks were obtained through hierarchical self-assembly as detected by SEM, TEM, and LSCM experiments. In particular, single bead-like chains were observed in the AFM and TEM images, which provided direct, visual evidence for the aggregation of positively charged metallacycles and negatively charged heparin. More interestingly, further optical study demonstrated that this TPE-decorated metallacycle could function as a turn-on fluorescent probe for heparin detection with high sensitivity and selectivity. Thus, this research presents the first example of counter polyanion-induced hierarchical self-assembly of discrete metallacycles and provides a "proof-of-principle" method for heparin sensing and binding.

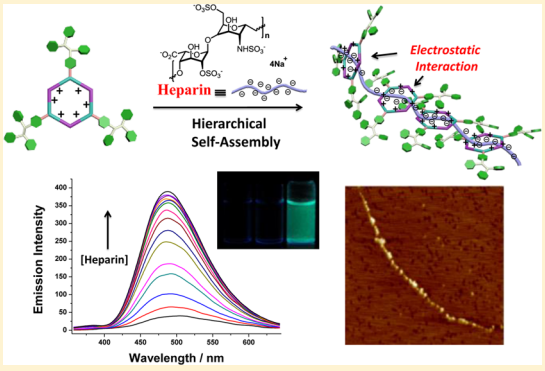

INTRODUCTION

Nature includes many elegant functional systems that are prepared from various simple precursors through multiple noncovalent interactions via hierarchical self-assembly.[1] A well-known example of hierarchical self-assembly is the formation of collagen, the primary component of connective tissue in mammals. Three polypeptide strands first twist into a right-handed triple helix, which subsequently self-assembles into microfibrils and then aggregates into larger collagen fibers.[2] Mimicking hierarchical self-assembly in artificial systems is a promising route toward obtaining sophisticated architectures with various structures and specific functionalities.[3] Thus, the investigation of hierarchical self-assembly for constructing artificial functional materials has attracted considerable attention from chemists in many subdisciplines.[4]

In recent decades, coordination-driven self-assembly has evolved into a well-established methodology for constructing well-defined, discrete metallosupramolecular structures, from two-dimensional (2-D) polygons to three-dimensional (3-D) cages, prisms, and polyhedra.[5,6] Recent investigations have demonstrated that properly attaching or incorporating func-

Received: June 24, 2015
Published: August 31, 2015

ACS Publications © 2015 American Chemical Society

DOI: 10.1021/jacs.5b06565
J. Am. Chem. Soc. 2015, 137, 11725−11735

tional moieties into or onto precursors does not hinder coordination-driven self-assembly, thus allowing the formation of functionalized supramolecular polygons or polyhedra.[7−9] In addition, because the formation of metal−ligand bonds can occur in parallel with other noncovalent interactions, such as hydrogen bonding, $\pi-\pi$ interactions, and van der Waals forces, the introduction of functional moieties that possess other noncovalent interactions as secondary driving forces to induce hierarchical self-assembly has evolved into a rational strategy for constructing functional materials involving discrete metallacycles. Very recently, a variety of functional materials, including metallohydrogels, amphiphilic nanostructures, and stimuli-responsive supramolecular polymers, have been successfully prepared by employing this strategy.[10,11] For example, we have demonstrated that the introduction of a pillar[5]arene functional group onto the dipyridine ligand allows the formation of multiple stimuli-responsive supramolecular polymer gels through hierarchical self-assembly.[10c] However, in these reported examples, research interests have focused on the peripheral functional groups that offer secondary driving forces during hierarchical self-assembly. The effect of the metallacycle itself has been ignored. It should be noted that the vast majority of self-assembled metallacycles themselves are highly charged because of the existence of nitrogen-donor ligands and oxidized metal ions.[5a−d] Therefore, we anticipated that the multiple positive charges of the metallacycle skeleton would provide an ideal platform for the construction of a novel, higher-order supramolecular architecture through hierarchical self-assembly via electrostatic interaction.

Electrostatic interaction, a widespread noncovalent interaction in nature, is of fundamental importance in determining the structure, dynamics, and function of biomolecules (e.g., protein folding, pH-induced conformational changes, and molecular recognition).[12] Self-assembly of simple precursors via electrostatic interactions has wide applications in the construction of complicated supramolecular architectures, including molecular capsules, monolayers, and helical nanoribbons, some of which exhibit promising potential in photonics, electronics, conducting polymers, and polyelectrolytes.[13] Stimulated by these successful examples, we envisioned that the construction of novel, higher-order supramolecular aggregates could be realized by properly selecting suitable negatively charged polymers to interact with positively charged metallacycles. Heparin is a linear, unbranched, sulfated polysaccharide that has been widely employed as an anticoagulant because it can effectively prevent the formation of blood clots.[14] Moreover, heparin is well-known for its high negative charge density due to the existence of sulfate and carboxylate groups within the main chain.[15] Thus, in this study, heparin was selected to investigate the hierarchical self-assembly involving positively charged metallacycles via electrostatic interaction.

To probe the hierarchical self-assembly process, an aggregation-induced emission (AIE) active unit, tetra-phenylethylene (TPE),[16] was introduced onto the metallacycle from a 120° TPE-containing dipyridine ligand via coordination-driven self-assembly. Note that the AIE effect has been extensively employed to monitor the progress of supramolecular aggregation since Tang's pioneering work in 2001.[17,18] Photophysical investigation of the TPE-based metallacycle revealed that the addition of heparin into the metallacycle solution resulted in dramatic fluorescence enhancement. Because TPE units typically exhibit enhanced emission in the aggregate state, the observed fluorescence enhancement supported the aggregation between the positively charged metallacycle and the negatively charged heparin, driven by multiple electrostatic interactions. In addition, the formation of entangled pearl-necklace networks through hierarchical self-assembly was indicated by SEM, TEM, and LSCM experiments. Further AFM and TEM study at low concentration revealed the existence of single bead-like chains, which provided direct proof for the formation of higher-order supramolecular aggregation driven by electrostatic interactions. This self-assembly behavior could be utilized to quantify heparin based on its emission spectral changes. The detection range (0−28 μM) covered the clinical dosage level. Moreover, a high selectivity to heparin over other mono- and disaccharides, even structurally similar analogues such as chondroitin 4-sulfate (ChS) and hyaluronic acid (HA), was achieved. It should be noted that the close monitoring and quantification of heparin is of pivotal importance in medical applications[19] because heparin overdose can cause numerous catastrophic complications, including hemorrhages and heparin-induced thrombocytopenia.[20] Therefore, we present the first example of counter polyanion-induced hierarchical self-assembly of discrete metallacycles driven by multiple electrostatic interactions and provide a new method to detect heparin with high sensitivity and selectivity.

RESULTS AND DISCUSSION

Synthesis and Characterization. The desired 120° TPE-containing donor building block **5** was synthesized through a three-step sequence as shown in Scheme 1. The Sonogashira coupling reaction of ethynyl-tetra-phenylethylene **1** and ((5-bromo-1,3-phenylene) bis(ethyne-2,1-diyl))bis-(trimethylsilane) **2**, followed by a deprotection reaction, generated the TPE-derived ((3,5-diethynylphenyl)ethynyl)-tetra-phenylethylene **4**. The subsequent Sonogashira coupling of **4** with 4-idopyridine yielded TPE-functionalized 120° donor ligand **5** in satisfactory yield in the presence of $Pd(PPh_3)_4$ and CuI as catalysts.

Scheme 1. Synthesis of 120° TPE-Functionalized Donor Ligand 5

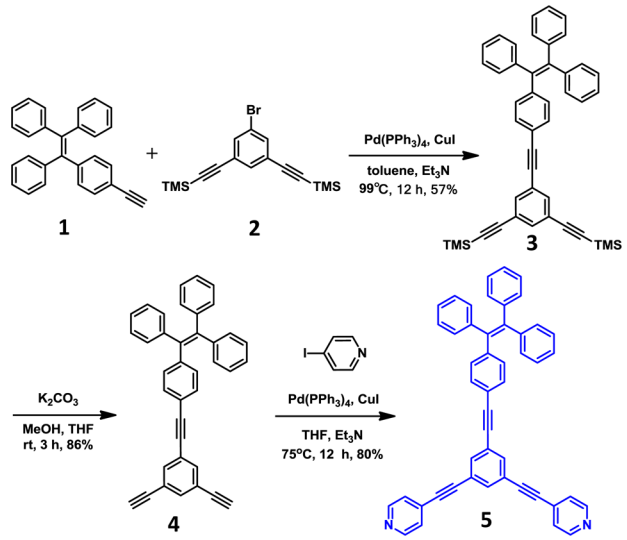

Tris-TPE hexagonal metallacycle **7** was prepared by stirring a mixture of 120° TPE-containing donor **5** and 120° diplatinum(II) acceptor **6** in a 1:1 ratio in CH_2Cl_2 (Scheme 2). Self-

DOI: 10.1021/jacs.5b06565
J. Am. Chem. Soc. 2015, 137, 11725−11735

Scheme 2. Self-Assembly of TPE-Containing 120° Donor 5 and Acceptor 6 into Tris-TPE Hexagonal Metallacycle 7

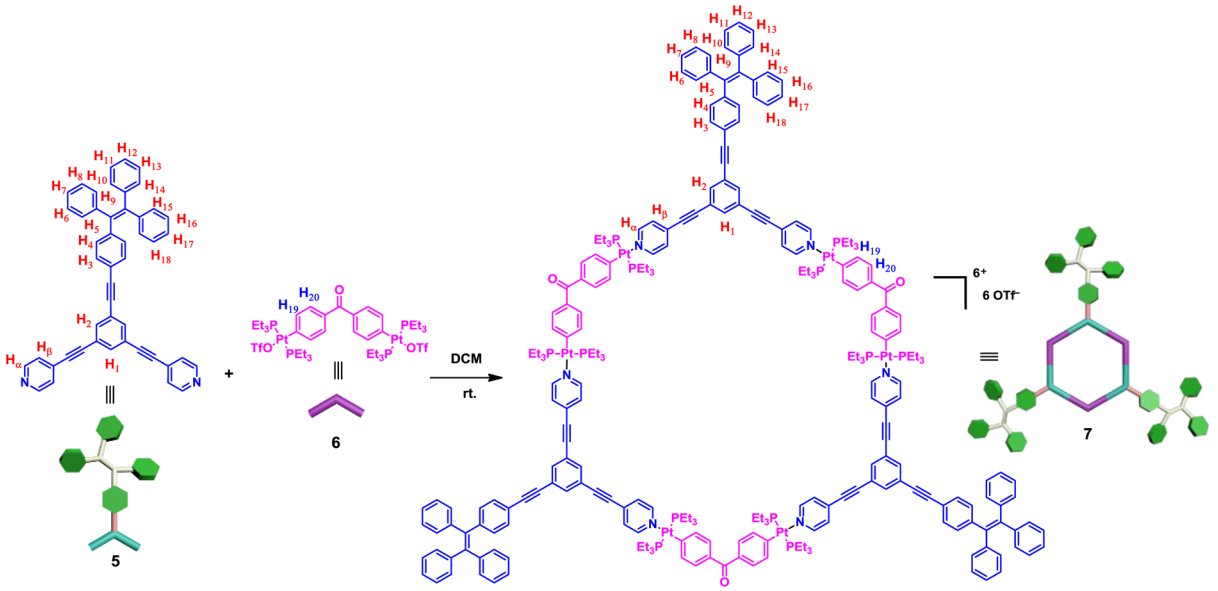

assembly of the two-component metallacycle **7** was monitored by multinuclear NMR spectroscopy. Analysis of the ^{31}P NMR spectrum (Figure 1) of the reaction solution was consistent

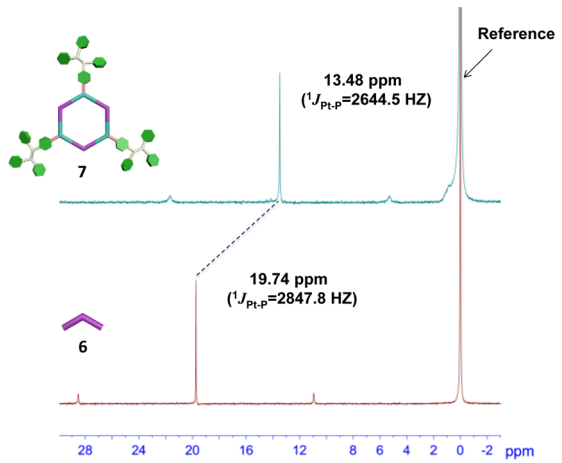

Figure 1. ^{31}P NMR spectra (161.9 MHz, in CD_2Cl_2, 298 K) of acceptor **6** (bottom) and tris-TPE metallacycle **7** (top).

with the formation of highly symmetric species. The appearance of a sharp singlet at ca. 13.5 ppm was observed, which was shifted by ca. 6.3 ppm upfield relative to the starting acceptor unit **6**. This change, as well as the decrease in the coupling of the flanking ^{195}Pt satellites (ca. $\Delta^1J_{P-Pt} = -203$ Hz), was consistent with the electron back-donation from the platinum atoms. Examination of the ^1H NMR spectrum (Figure 2) also indicated the existence of a highly symmetric structure. The ^1H NMR spectrum exhibited significant downfield shifts of pyridyl proton signals (for the α proton, ca. $\Delta\delta = 0.10$ ppm; for the β proton, ca. $\Delta\delta = 0.46$ ppm) associated with the loss of electron density upon coordination of the nitrogen atom with platinum metal centers. The sharp NMR signals in both the ^{31}P and ^1H NMR spectra, along with the solubility, ruled out the formation of oligomers. Further characterization by two-dimensional spectroscopic techniques (2-D $^1H-^1H$ NOESY), in which the presence of cross peaks between the signals of the

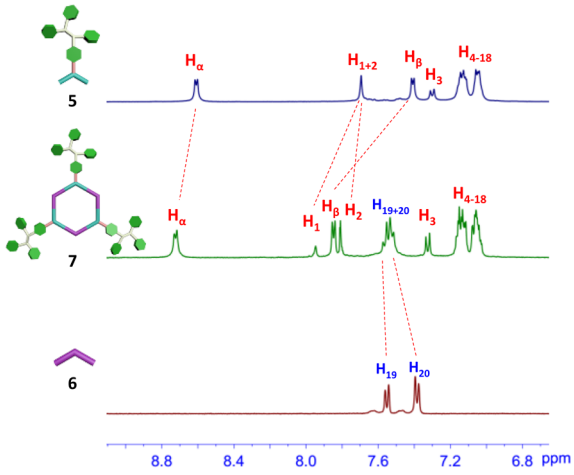

Figure 2. Partial ^1H NMR spectra (400 MHz, in CD_2Cl_2, 298 K) of acceptor **6** (bottom), 120° dipyridine donor **5** (top), and tris-TPE metallacycle **7** (middle).

pyridine protons (α-H and β-H) and the PEt_3 protons ($-CH_2$ and $-CH_3$) were observed (Figure S1), was in agreement with the formation of the discrete tris-TPE hexagonal metallacycle **7** based on the formation of N–Pt bonds.

Investigation of the electrospray ionization mass spectrometry (ESI-TOF-MS) provided further support for the existence of TPE-functionalized metallacycle **7**. As shown in Figure 3, the

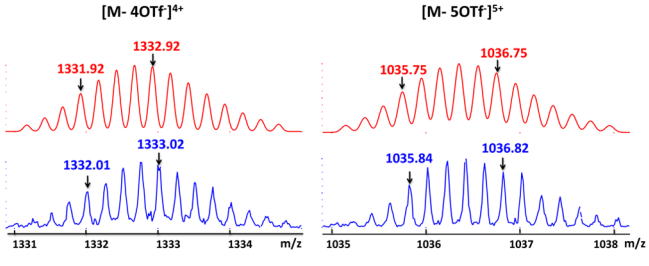

Figure 3. Theoretical (top) and experimental (bottom) ESI-TOF-MS spectrum of tris-TPE hexagonal metallacycle **7**.

DOI: 10.1021/jacs.5b06565
J. Am. Chem. Soc. 2015, 137, 11725–11735

mass spectrum of 7 exhibited two main peaks at m/z = 1036 and m/z = 1333, corresponding to different charge states resulting from the loss of trifluoromethanesulfonate counterions $[M-5OTf^-]^{5+}$ and $[M-4OTf^-]^{4+}$, respectively, where M represents the intact assembly. The isotopic resolution of each peak was consistent with the theoretical distribution, which allowed for the molecularity of the tris-TPE hexagonal metallacycle to be unambiguously established.

All attempts to grow X-ray single crystals of 7 have thus far proven unsuccessful. Therefore, molecular simulation using the PM6 semiempirical molecular orbital method was conducted to gain further insight into the structural characteristics of tris-TPE metallacycle 7. Molecular simulation indicated that metallacycle 7 featured a roughly planar hexagonal ring at the core surrounded by three rigid TPE units with an internal diameter of 3.0 nm (Figure S2a). Moreover, transmission electron microscopy (TEM) was performed to visualize the size and shape. A very dilute solution of 7 (~10 nM) was deposited onto copper grids, followed by slow evaporation in air at room temperature to prepare the TEM samples. The obtained TEM images (Figure S2b) exhibited discrete particles with a measured diameter of ~3.0 nm, which was comparable to the theoretical size. In order to obtain further structural information on tris-TPE metallacycle 7, the diffusion coefficient (D) of metallacycle 7 was determined by two-dimensional diffusion-ordered NMR (DOSY) experiment. A distinct band at log D = −9.80 (Figure S3) was observed, suggesting formation of single product. Moreover, the diameter of metallacycle 7 was calculated to be 4.5 nm on the basis of the Stokes−Einstein equation, which was in good agreement with the modeling result.

Photophysical Investigation of Tris-TPE Hexagonal Metallacycle 7. The self-assembled metallacycle 7 was soluble in common organic solvents, such as dichloromethane, acetone, chloroform, and THF, but was insoluble in water and some nonpolar solvents, such as hexane. Thus, the optical properties of the tris-TPE metallacycle 7 were first evaluated in the mixed solvent of CH_2Cl_2/hexane. The dilute CH_2Cl_2 solution of metallacycle 7, as expected, exhibited very weak luminescence. With the addition of hexane, the emission of metallacycle 7 in the mixed solvents remained as faint as it had been in the original CH_2Cl_2 solution when the hexane fraction was below 60%. However, upon continuing to increase the hexane content to 100%, the fluorescence intensity with the emission maximum at 486 nm abruptly increased (Figure 4b). For example, when the hexane content was increased from 60% to 100%, the emission intensity value increased to 495, which was approximately 10-fold higher than that of its molecularly dispersed species in the 60% hexane. As shown in Figure 4c, an obvious enhancement of the emission intensity with increase of hexane fraction was observed upon excitation at 365 nm using an ultraviolet lamp. The UV absorption spectra of 7 in the CH_2Cl_2/hexane mixture were also measured. A level-off tail that is commonly observed in nanoparticle suspensions[21] was observed in the visible spectral region with a hexane fraction up to 60%, and it further intensified as the hexane fraction increased (Figure 4a). These findings were strongly indicative that metallacycle 7 decorated with three TPE moieties was AIE-active. Note that the TPE-containing precursor **5** was not AIE-active in the mixture solvents of CH_2Cl_2/hexane and exhibited weak emission at 398 nm (Figure S4).

Dynamic light scattering (DLS) measurement of metallacycle 7 was performed to further investigate the aggregation process

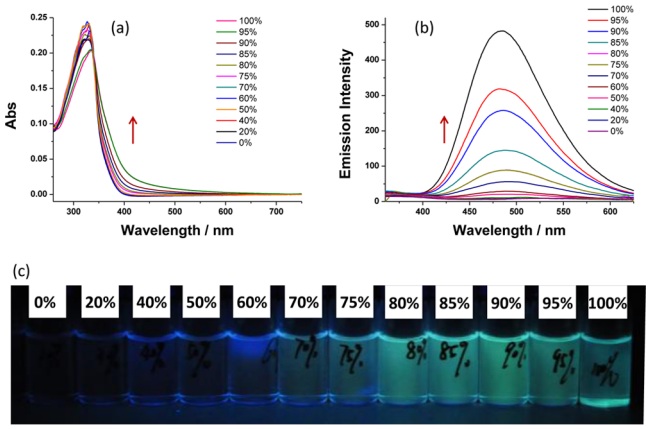

Figure 4. Absorption (a) and fluorescence emission spectra (b) of tris-TPE hexagonal metallacycle 7 versus the hexane fraction in the CH_2Cl_2/hexane mixtures (λ_{ex} = 330 nm, c = 1.0 μM). (c) The photographs of tris-TPE hexagonal metallacycle 7 in CH_2Cl_2/hexane mixtures with different fractions of hexane on excitation at 365 nm using an ultraviolet lamp at 298 K (c = 1.0 μM).

at different hexane contents. As shown in Figure S5, when the hexane content increased from 60 to 90%, the average hydrodynamic diameters (D_h) exhibited a gradual increase from 81.3 to 512 nm, which indicated a gradual aggregation process. Furthermore, TEM investigation was conducted to further study the morphology of the obtained aggregates. No regular morphology was observed in mixture solvents with low hexane content (0−50%). When the hexane fraction was above 60%, regular nanoparticles were observed, and the diameter data exhibited a slight increase along with the increase of the hexane fraction (60−80%, Figure S6a−c). Such regular nanospheres were further gathered to form bead-like structures that converted into cross-linking bead microstructures at higher hexane contents (85−100%, Figure S6d−f). A similar morphology transformation (Figure S7) was observed in the scanning electron microscope (SEM) images, which was consistent with the solvent-induced aggregation process observed in the DLS and TEM tests.

Hierarchical Self-Assembly of Metallacycle with Heparin Driven by Multiple Electrostatic Interactions. Because the self-assembled tris-TPE metallacycles are positively charged due to the use of neutral nitrogen-donor ligands with oxidized metal ions, it is possible to perform hierarchical self-assembly upon the addition of the negatively charged polymer via electrostatic interaction. Heparin, an anticoagulant drug used in surgery and the treatment of thrombotic diseases, is a highly sulfated polysaccharide with high, negatively charged density resulting from many sulfate and carboxylate groups in the chain. Thus, heparin was employed to investigate the hierarchical self-assembly of tris-TPE hexagonal metallacycle 7 driven by multiple electrostatic interactions.

Because heparin is not soluble in common organic solvents, such as dichloromethane, the mixed solvent of acetone and water was employed to perform the following study. As shown in Figure 5, with the slow addition of heparin (0−50 μg) into a solution (acetone/H_2O 30/70, v/v) of metallacycle 7 (10 μM), a gradual fluorescence enhancement at approximately 486 nm was observed in the emission spectra. The observed enhancement of the fluorescence intensity was attributed to the aggregation of TPE moieties because the maximum emission wavelength was consistent with the previous optical study. The

DOI: 10.1021/jacs.5b06565
J. Am. Chem. Soc. 2015, 137, 11725−11735

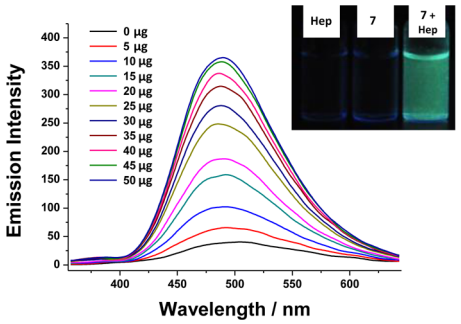

Figure 5. Emission spectral changes of 7 (10 μM) with the addition of heparin. Inset: the photographs of heparin (left), tris-TPE hexagonal metallacycle 7 (middle), and their mixture (right) upon excitation at 365 nm using an ultraviolet lamp at 298 K.

heparin itself is emission-inert in all detection ranges. This result provided strong support that electrostatic interactions between the rigid, positively charged metallacycle 7 and the flexible, negatively charged heparin chain moved the hexagonal metallacycle into close proximity and induced the hierarchical self-assembly. To prove that the electrostatic interaction is critical for such an assembly process, a controlled experiment was performed using TPE-containing ligand **5** under the same conditions. No significant fluorescence change was observed upon the addition of heparin into the solution (acetone/H_2O 30/70, v/v) of ligand **5** (30 μM, Figure S8).

DLS experiments were performed to investigate the aggregation process. After adding (10 μg) heparin into the solution of 7 (10 μM), the average D_h was found to be 221 nm, which was larger than that of heparin (30 nm). Moreover, when the concentration of metallacycle 7 was increased to 30 μM, the average D_h of aggregation measured by DLS increased to 367 nm after the addition of 10 μg heparin (Figure S9). This phenomenon indicated that the aggregation of metallacycle 7 occurred upon the addition of heparin.

The formation of aggregates from metallacycle 7 and heparin was directly observed using SEM. Cross-linked three-dimensional (3-D) networks were found in the SEM images for the solution of tris-TPE hexagonal metallacycle 7 (10 μM) containing 10 μg heparin (Figure 6a and S10). The entangled bulky pearl-necklace networks with the larger size (Figure S11) were formed upon increasing the concentration of metallacycle 7 to 30 μM and the amount of heparin to 30 μg. To gain further insight into the elemental composition of these aggregate structures, investigation by employingenergy dispersive X-ray spectroscope (EDX) was performed. The elemental compositions of carbon, oxygen, fluorine, sulfur, platinum, and phosphorus were measured in the aggregates (Figure 6b), which strongly suggested that these entangled pearl-necklace networks were generated from heparin-induced hierarchical self-assembly of metallacycle 7. Further morphological investigation of the obtained aggregates from metallacycle 7 (10 μM) and heparin (10 μg) using TEM was performed. Similar pearl-necklace network structures (Figure 6c and S13) were observed in the TEM images, which was consistent with the discovery in the SEM studies. More intuitively, blue luminescence was emitted from the network structures, which was directly observed by laser scanning confocal microscopy (LSCM) images, as exhibited in Figure 6d and S14. These results demonstrated that the aggregates were generated from the hierarchical self-assembly of tris-TPE metallacycle 7 with the addition of heparin. Note that only

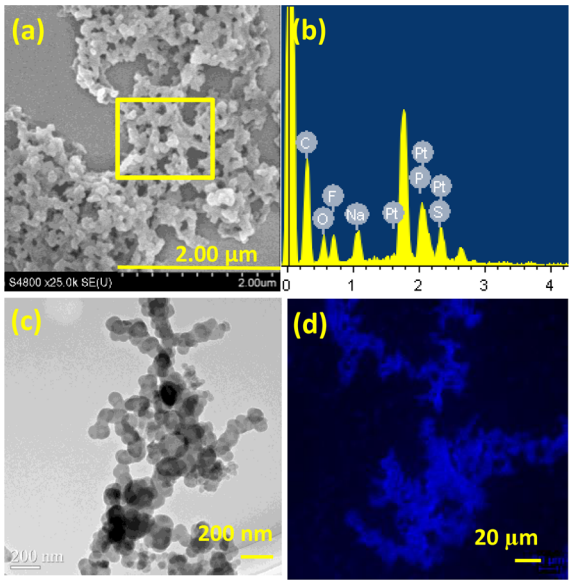

Figure 6. SEM images of 7 and heparin composites (a, the scale bar is 2.0 μm); the EDX results of 7 and heparin composites collected from the area marked by the pink boxes (b); TEM images of 7 and heparin composites (c, the scale bar is 200 nm); and LSCM images of 7 and heparin composites (d, λ_{ex} = 405 nm).

regular micelle structures with a diameter of ca. 30 nm rather than pearl-necklace networks were observed in AFM, TEM, and SEM images of the mixture of TPE-containing ligand **5** and heparin (Figure S23).

To obtain more structural evidence and a better understanding of the interaction between tris-TPE metallacycle 7 and heparin, atomic force microscopy (AFM) measurements in very dilute solution (~10 nM) were conducted to directly visualize the sizes and shapes of metallacycle 7, heparin, and the 7-heparin composites. As presented in Figure 7a,b and S15a,d, dot morphology with a height value of approximately 3.4 nm (Figure 7c) was observed for tris-TPE hexagonal metallacycle 7 in the AFM images, which was similar to the theoretical size and the TEM results. For heparin, a helical belt morphology with different lengths was observed (Figure 7d,e and S15b,e). The height with an average value of 1.0 nm (Figure 7f) was obtained by measuring different areas. When dropping a very dilute solution of the mixture of tris-TPE metallacycle 7 and heparin on a freshly cleaved mica surface, some single bead-like chains were observed, as shown in Figure 7g–h and Figure S16.

The height profile of the bead-like polymers had a height distribution ranging between approximately 1.0 and 4.0 nm (Figure 7i). The height profile of the depressed part was comparable to the typical height of heparin, and the hump area's height profile was slightly higher than that of metallacycle 7. Thus, the formation of the bead-like morphology was attributed to the complexation of metallacycle 7 with the heparin polymer belt driven by electrostatic interactions. Similar single chains were also obtained in the TEM measurements of the dilute solution (~10 nM for 7) of the mixture of metallacycle 7 and heparin (Figure S19 and S20).

In order to obtain the further insight into the hierarchical self-assembly process, the concentration-dependent AFM, TEM, and SEM investigation on aggregation morphology of 7-heparin complex was carried out. For instance, upon increasing the concentration from 0.01–1.0 mM, the concentration-dependent AFM measurement revealed that

DOI: 10.1021/jacs.5b06565
J. Am. Chem. Soc. 2015, 137, 11725–11735

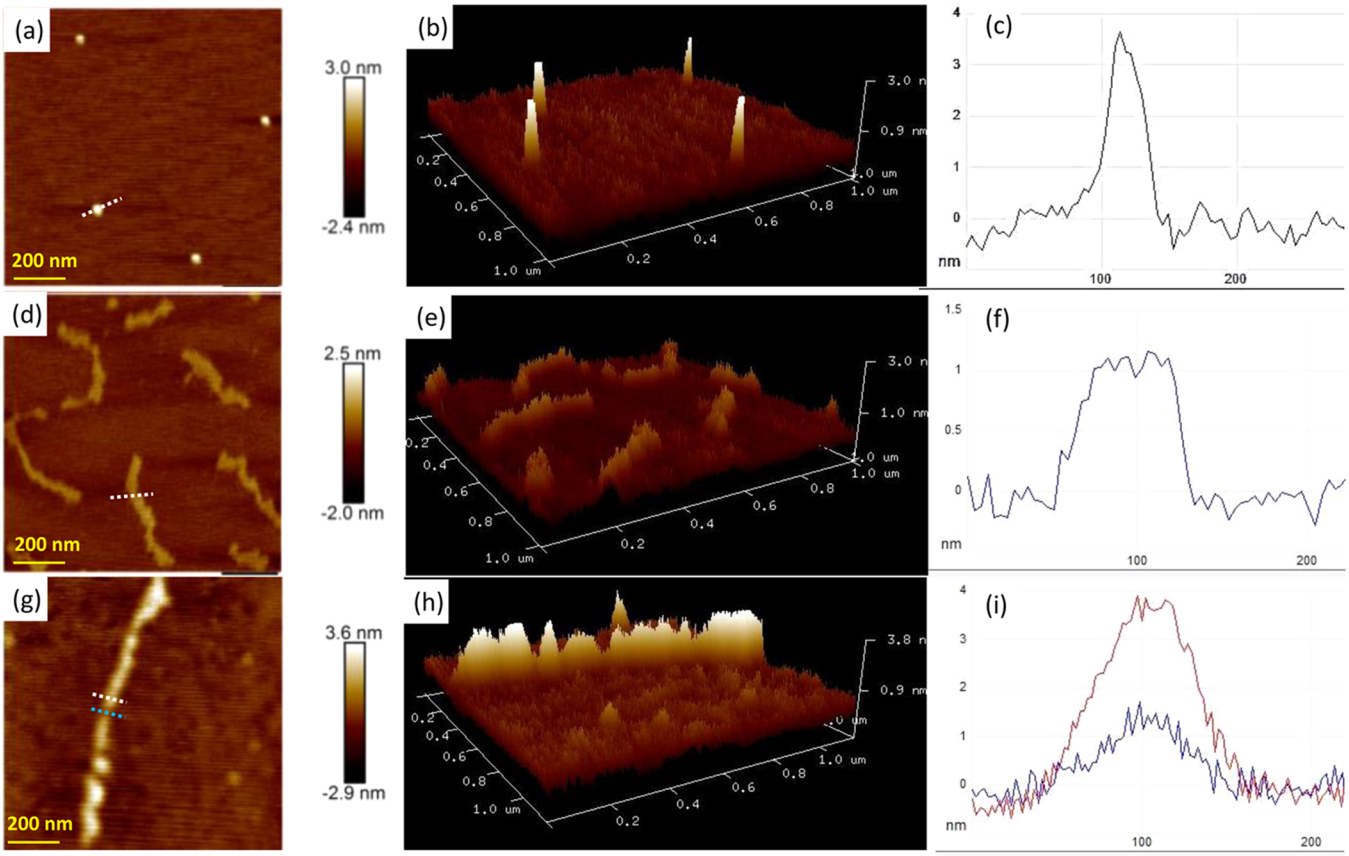

Figure 7. AFM height images, 3-D images and the corresponding height profiles as indicated by lines of very dilute solutions of tris-TPE hexagonal metallacycle 7 (a,b,c), heparin (d,e,f), and a mixture of tris-TPE hexagonal metallacycle 7 and heparin (g,h,i).

the bead-like structure gradually entangled with each other to form cross-linked necklace structures, which were further intertwined to form dense pearl-necklace networks (Figure S18). The similar transformation from single bead-like chain into the entangled pearl-necklace networks was observed in concentration-dependent TEM and SEM images as well (Figure S22 and S12).

Furthermore, the multinuclear NMR (^{1}H and ^{31}P) measurement of 7-heparin complex was performed to gain the better understanding of the interaction bewteen tris-TPE metallacycle 7 and heparin. It was found that, with the addition of heparin, the proton signals around Pt−N bonds (e.g., pyridine protons (α-H and β-H) and PEt_3 protons ($-CH_2$ and $-CH_3$)) displayed an obvious upfield shift as shown in Figure S24a. For example, α-H protons on pyridine displayed 0.08 ppm upfield shift. In addition, for CH_2 protons in PEt_3, an upfield shift of 0.06 ppm was observed. It should be noted that, for other proton signals far away from Pt−N bonds, nearly no chemical shift was observed. The ^{31}P NMR signal also exhibited an upfield shift (ca. $\Delta\delta$ = 0.07 ppm) upon the introduction of heparin (Figure S24b). These observed upfield shifts were associated with the increase of electron density upon the addition of heparin, which indicated that electrostatic interactions between positively charged tris-TPE metallacycle 7 and negatively charged heparin occurred around the Pt−N moieties.

To better understand the interaction between the positively charged metallacycle 7 and the negatively charged heparin, PM6 semiempirical molecular orbital method was employed to obtain the optimized geometry of heparin and the possible binding modes between metallacycle 7 and heparin. The molecular simulation disclosed the diameter of heparin to be around 1.2−1.6 nm (Figure S25), which is smaller than the internal diameter of metallacycle 7 (3.0 nm). This finding indicated that the polymer chain of heparin could pass through the ring of 7. In addition, analysis of the five typical possible binding modes between metallacycle 7 and heparin (Figure 8 and Figure S26−S30) suggested that the skew-crossing mode (with the lowest energy of −6461.02 kcal/mol, Table S1) might be the dominant manner rather than center-crossing mode (with energy of −6369.13 kcal/mol) when the electrostatic

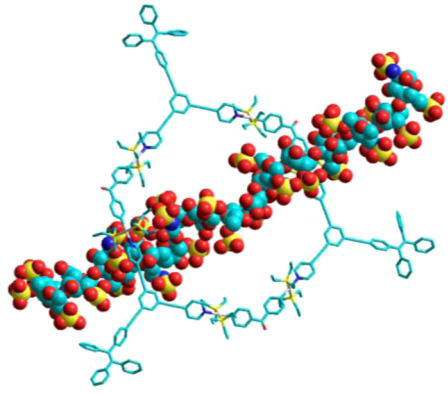

Figure 8. Simulated molecular model of skew-crossing mode with heparin shown in space-filling mode and 7 shown in ball-and-stick mode optimized by PM6 semiempirical molecular orbital method.

DOI: 10.1021/jacs.5b06565
J. Am. Chem. Soc. 2015, 137, 11725−11735

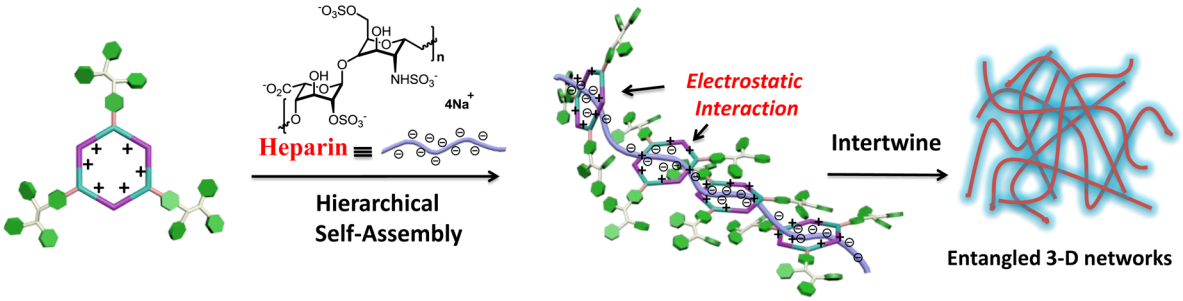

Figure 9. Schematic representation of the possible binding and aggregation mode of tris-TPE metallacycle **7** and heparin.

interactions between metallacycle **7** and heparin occurred. However, it is very difficult to rule out other possible ways such as skew-clinging or side-crossing modes (with energy of −6450.77 kcal/mol and −6446.02 kcal/mol, respectively) since the calculated energy was close to that of skew-crossing mode. It is worth to mention that there are still some untouched interaction sites available on the metallacycle after it interacted with one heparin polymer chain, thus making it possible for further intertwining with the other polymer chain to produce the entangled networks.

On the basis of the above experimental and theoretical results, we propose a possible binding and aggregation mode for metallacycle **7** and heparin (Figure 9). First, the positively charged hexagonal skeleton anchored metallacycle **7** to heparin through electrostatic interactions of the positively charged metallacycle skeleton with the negatively charged $-COO^-$ and $-OSO_3^-$ groups of the two terminal tetrasaccharide sugars, leading to the metallacycle orienting and organizing along the polysaccharide chain. The other groups on both the metallacycle and heparin were then brought into close contact. The flexibility of the polysaccharide chain and the untouched interaction sites available on metallacycle resulted in the intertwining of the polymer chain to produce entangled 3-D networks. Such networks further entangled with each other at high concentrations, allowing the generation of bulky pearl-necklace network microstructures. Although it is still very difficult to demonstrate the actual process of formation of such higher-order supramolecular structures, there is no doubt that electrostatic interactions played critical roles during the formation of the ordered aggregates due to the extensive charge complementarity between metallacycle **7** and heparin.

To further understand the impact of the positively charged metallacycle skeleton on the hierarchical self-assembly and aggregation process, a model organometallic complex **9** was prepared (Scheme 3 and S3), in which 120° TPE-containing ligand **5** was coordinated with two mono-Pt(II) acceptor units **8**. The formation of the model structure **9** was confirmed by multinuclear NMR (^1H and ^{31}P) spectra and CSI-TOF-MS spectrometry (Figure S31, S32 and S33). Although a gradual fluorescence enhancement at approximately 486 nm was observed in the emission spectra (Figure S34a) with the slow addition of heparin (0−30 μg) to a solution (acetone/H_2O 30/70, v/v) of model complex **9** (30 μM), the intensity enhancement was much weaker than that with metallacycle **7** (Figure S34b). Furthermore, the morphology for the mixture of mono-TPE model complex **9** and heparin were found to be short rod, which were also different from the morphology obtained from the **7**-heparin complex (Figure S35). This phenomenon indicated that the positively charged metallacycle skeleton provided an ideal platform to undergo hierarchical self-assembly with negatively charged heparin driven by electrostatic interactions.

Turn-on Selective Probe for Heparin Detection. As demonstrated above, the TPE functionalized metallacycle **7** exhibited heparin-induced aggregation behavior accompanied by an obvious emission enhancement. Heparin has long been used as an anticoagulant to convert antithrombin into a suicide substrate for procoagulant proteinase. Close monitoring of heparin levels is of vital importance during anticoagulant therapy and surgery because an overdose of heparin could cause catastrophic complications, such as hemorrhages and heparin-induced thrombocytopenia.[20] We envisioned that this tris-TPE metallacycle **7** could be employed as a fluorescent probe for the quantification of heparin based on its spectral change. As shown in Figure 10, with the addition of heparin, the emission intensity of metallacycle **7** continued to linearly increase until the concentration of heparin reached 28 μM, after which the emission increase slowed. This finding suggested that calibrating the heparin concentration based on the first concentration stage (0−28 μM) is practical.

To eliminate the discrepancy across the different original emission intensities and optical collection conditions, the net

Scheme 3. Construction of Mono-TPE Model Complex 9

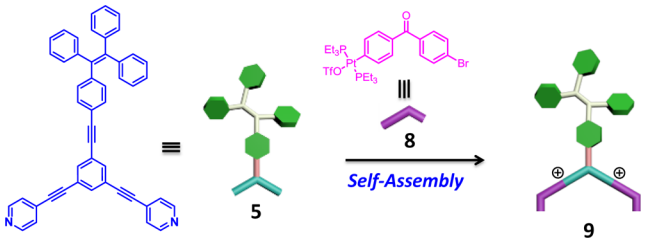

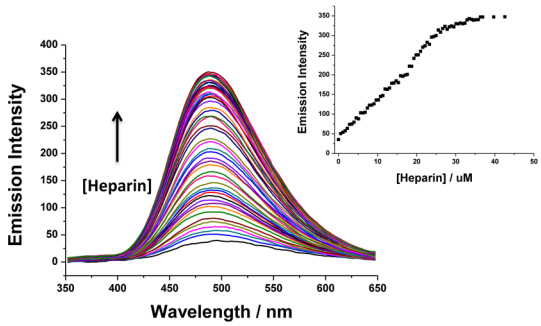

Figure 10. Emission spectral changes of **7** (10 μM) with increasing concentration of heparin. Insets: plots of the relative emission intensity at 486 nm with various concentrations of heparin.

DOI: 10.1021/jacs.5b06565
J. Am. Chem. Soc. 2015, 137, 11725−11735

increase value $[(I - I_0)/I_0]$, was used as a function of analyte concentration, where I and I_0 are the maximum intensities with and without analyte, respectively. Thus, a linear relationship was obtained for the concentration range from 0 to 28 μM for measurements (Figure 11, blue line) with a slope of the curve

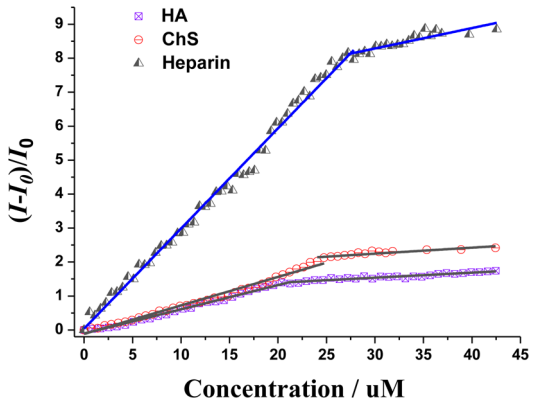

Figure 11. $(I - I_0)/I_0$ values as a function of the concentrations of heparin, ChS, and HA.

of 0.294 L/mol and a standard error of 0.003 L/mol. Because the heparin concentrations at the therapeutic dosage level are 0.2−1.2 U/mL (1.7−10 μM) in postoperative and long-term care, the linear detection range of this assay, corresponding to 0−28 μM, covered the range of heparin detection required in clinical applications.

In order to investigate the influence of solvent to the change of fluorescence emission, a control experiment was performed, in which the blank solvent mixture rather than heparin was added into the solution of tris-TPE metallacycle 7 (Figure S36). Almost no change of the net increase value of $(I - I_0)/I_0$ was observe with the addition of blank solvent, indicating that the observed emission increase with the addition of heparin into the tris-TPE metallacycle 7 was mainly caused by the heparin-induced aggregation.

To examine the selectivity of metallacycle 7 toward heparin, the fluorescence spectra of 7 were recorded with the addition of possible interfering biomolecules, including mono- and disaccharides, such as glucose and sucrose, and serum albumins. Among these biomolecules, only the addition of heparin resulted in an intensive increase in the emission intensity, indicating the good selectivity of metallacycle 7 toward heparin (Figure 12). Moreover, structurally similar glycosaminoglycans analogues, such as chondroitin 4-sulfate (ChS) and hyaluronic acid (HA) (Figure S37−38), which are commonly regarded as contaminants for clinical heparin, were also chosen for control experiments. Under the same conditions, the addition of HA or ChS into the solution of 7 led to less fluorescence increase compared with heparin, as shown in Figure 11. The slopes of the increasing $[(I - I_0)/I_0]$ values for heparin, ChS, and HA were 0.294, 0.0706, and 0.0689 L/mol, respectively, which indicated that metallacycle 7 featured excellent selectivity for heparin.

In order to investigate electrostatic interaction of tris-TPE metallacycle 7 with other highly charged polymers, poly(acrylic acid) sodium (PAAS) and poly(sodium-*p*-styrenesulfonate) (PSS) were employed for selectivity analysis. As indicated in chemical structure of PAAS (Figure S39a) and PSS (Figure S40a), they are both highly charged polymers with similar negatively charged moieties of heparin although the main

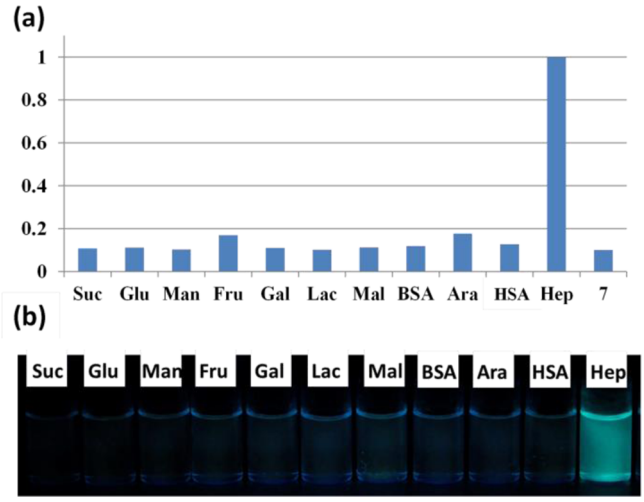

Figure 12. Selectivity analysis (a) and photos (b) with various possible interfering biomolecules. Suc = sucrose, Glu = glucose, Man = mannose, Fru = fructose, Gal = galactose, Lac = lactose, Mal = maltose, BSA = bovine serum albumin, Ara = arabinose, HSA = human serum albumin, Hep = heparin, and 7 = metallacycle 7.

backbone of polymer chain is different from heparin. Compared to heparin, less fluorescence increase was observed when the negatively charged polymers PAAS or PSS was added into the solution of tris-TPE metallacycle 7 as shown in Figure S41 and Figure S42. Furthermore, the slopes of the increasing $[(I - I_0)/I_0]$ values for PAAS and PSS were found to be 0.04 and 0.08 L/mol, respectively, which were much smaller than that of heparin (0.294 L/mol). These findings indicated that the tris-TPE metallacycle 7 also displayed good selectivity for heparin detection when compared with some other highly charged polymers. In order to understand such selectivity toward heparin, molecular simulation of the geometry of PAAS and PSS was performed, which revealed that the diameter of heparin (1.2−1.6 nm, Figure S25) was between the diameter of PAAS (0.6−0.8 nm, Figure S39b) and PSS (1.4−1.7 nm, Figure S40b). Thus, in this study, the structural effects such as size, functional groups, or molecular conformation played a non-negligible role during the host−guest recognition although electrostatic interaction was believed to be the main driving force.

Protamine sulfate, a highly cationic polypeptide, has been widely employed as a clinical antagonist for heparin because of its high binding affinity for heparin.[22] Thus, comparison of the binding affinity toward heparin between metallacycle 7 and protamine sulfate was performed. Upon the addition of protamine sulfate into the solution of 7-heparin composites, the intensity of the emission band at 486 nm remained steady in the emission spectra of the 7-heparin complexes (Figure S43). This unexpected result indicated that tris-TPE metallacycle 7 had stronger binding affinity for heparin than protamine sulfate.

CONCLUSIONS

Here, we present the first study of the hierarchical self-assembly of discrete, positively charged metallacycles with linear, negatively charged polysaccharides driven by multiple electrostatic interactions. With the aim of illustrating the hierarchical self-assembly process, the AIE active moiety TPE was introduced onto metallacycles. The obtained tris-TPE metalla-

DOI: 10.1021/jacs.5b06565
J. Am. Chem. Soc. 2015, 137, 11725−11735

cycle was characterized by 1-D multinuclear NMR (^{1}H and ^{31}P), 2-D NOESY, DOSY, and ESI-TOF-MS. Molecular simulation using PM6 semiempirical molecular orbital methods revealed that this TPE-decorated metallacycle featured a roughly planar hexagonal ring with a diameter of 3.0 nm.

By taking advantage of the electrostatic interaction between the positively charged metallacycle and the negatively charged heparin, higher-order aggregates were obtained with the addition of heparin into the solution of tris-TPE metallacycle. The obtained metallacycle-heparin aggregates exhibited typical AIE behavior, which supported the self-assembly of the metallacycle with heparin driven by electrostatic interaction. Morphology investigation by SEM, TEM, and DLS revealed that entangled pearl-necklace aggregation was formed through hierarchical self-assembly driven by multiple electrostatic interactions. In particular, the AFM and TEM study at low concentration provided direct proof for the formation of single bead-like chains during the hierarchical self-assembly of metallacycles with the addition of heparin. Both TPE-containing building block **5** and model complex **9** with two positive charges were employed to study their interaction with heparin. Optical study indicated that the existence of the positively charged metallacycle skeleton played a vital role during the aggregation process.

Because the aggregation process occurred with an obvious emission intensity change, further optical study indicated that tris-TPE metallacycle **7** could serve as a turn-on sensing probe for the quantification of heparin. The detection range was 0−28 μM, which covers the clinical dosage level. Moreover, the selectivity of metallacycle **7** to heparin was promising, even in comparison with structurally similar analogues, such as ChS and HA. Competitive binding tests revealed that metallacycle **7** exhibited stronger binding ability toward heparin than protamine sulfate, which has been widely used as an antagonist for heparin. Although some polyelectrolytes containing AIE moieties have been prepared and successfully employed as heparin sensors,[23] to the best of our knowledge, tris-TPE metallacycle **7** served as the first example of discrete metallosupramolecular architecture as heparin sensor derived from coordination-driven self-assembly. The inherent merits of coordination-driven self-assembly, including fast and facile construction of the final products, intrinsic internal cavities with tunable sizes and shapes as well as reversible disassembly and reassembly toward the external stimulus, allow coordination metallacycles to be good candidates for large biomolecule detection. In a word, this study presents the first example of counter polyanion-induced hierarchical self-assembly of a discrete metallacycle driven by electrostatic interaction, which not only enriches the library of functional metallacycles and expands the application of hierarchical self-assembly of discrete metallacycles, but also provides a promising "proof-of-principle" method for large biomolecules sensing and binding.

EXPERIMENTAL SECTION

Full experimental details are provided in the Supporting Information. The most important information is summarized briefly below.

Synthesis of 7. The dipyridyl donor ligand **5** (9.32 mg, 14.6 μmol) and the organoplatinum 120° acceptor **6** (19.33 mg, 14.6 μmol) were weighed accurately into a glass vial. To the vial was added 2.0 mL DCM, and the reaction solution was stirred at room temperature for 2 h to yield a homogeneous yellow solution. Pale yellow solid product **7** was obtained by removing the solvent under a vacuum. Yield: 40.83 mg, > 99%. ^{1}H NMR (CD_2Cl_2-*d*, 400 MHz) δ 8.73 (d, 4H, J = 5.6 Hz), 7.95 (s, 1H), 7.85 (d, 4H, J = 6.4 Hz), 7.81 (d, 2H, J = 1.2 Hz) 7.51−7.57 (m, 8H) 7.33 (d, 2H, J = 8.4 Hz) 7.05−7.16 (m, 19H), 1.37−1.38 (br, 24H), 1.13−1.17 (m, 36H). ^{31}P NMR (CD_2Cl_2-*d*, 161.9 MHz) δ 13.48 (s, J_{Pt-P}= 2644.5 Hz); ESI-MS m/z 1036.26 [M − 5OTf$^-$]$^{5+}$, 1331.92 [M − 4OTf$^-$]$^{4+}$.

SEM, TEM, EDX, AFM, and DLS Experiments. SEM images were obtained using an S-4800 (Hitachi Ltd.) with an accelerating voltage of 3.0−10.0 kV. Samples were prepared by dropping solutions onto a silicon wafer. To minimize sample charging, a thin layer of Au was deposited onto the samples before SEM examination. TEM images were recorded on a Tecnai G^2 F30 (FEI Ltd.). The sample for the TEM measurement was prepared by dropping the solution onto a carbon-coated copper grid. EDX measurements were performed using an S-4800 (Hitachi Ltd.) with a voltage of 10.0 kV. AFM images were obtained on a Dimension FastScan (Bruker) using ScanAsyst mode under ambient conditions. Scanasyst-Fluid+ probes were used for the scan. The AFM samples were prepared by dropping solutions onto a mica sheet. DLS measurements were performed under a Malvern Zetasizer Nano-ZS light scattering apparatus (Malvern Instruments, U.K.) with a He−Ne laser (633 nm, 4 mW).

UV−Vis Absorption and Fluorescence Emission Spectra. UV−vis spectra were recorded in a quartz cell (light path 10 mm) on a Cary 50Bio UV−visible spectrophotometer. Steady-state fluorescence spectra were recorded in a conventional quartz cell (light path 10 mm) on a Cary Eclipse fluorescence spectrophotometer.

Laser Scanning Confocal Microscopy Experiments. LSCM imaging was performed with an OLYMPUS ZX81 laser scanning microscope and a 60x oil-immersion objective lens. A 405 nm laser was selected as the excitation source.

ASSOCIATED CONTENT

Supporting Information

The Supporting Information is available free of charge on the ACS Publications website at DOI: 10.1021/jacs.5b06565.

Synthesis, characterization, and other experimental details. (PDF)

AUTHOR INFORMATION

Corresponding Author

*hbyang@chem.ecnu.edu.cn

Notes

The authors declare no competing financial interest.

ACKNOWLEDGMENTS

This work was financially supported by the 973 Program (No. 2015CB856600), NSFC/China (Nos. 21322206 and 21132005), and the Key Basic Research Project of Shanghai Science and Technology Commission (No. 13JC1402200). X. L. acknowledges the support of the National Science Foundation (CHE-1506722) and PREM Center for Interfaces (DMR-1205670)

REFERENCES

(1) Babloyantz, A. *Molecules, Dynamics, and Life: An Introduction to Self-Organization of Matter*; John Wiley & Sons: New York, 1986.
(2) Prockop, D. J.; Fertala, A. *J. Struct. Biol.* **1998**, *122*, 111−118.
(3) Elemans, J. A. A. W.; Rowan, A. E.; Nolte, R. J. M. *J. Mater. Chem.* **2003**, *13*, 2661−2670.
(4) (a) Choi, I. S.; Bowden, N.; Whitesides, G. M. *Angew. Chem., Int. Ed.* **1999**, *38*, 3078−3081. (b) Davis, J. T.; Spada, G. P. *Chem. Soc. Rev.* **2007**, *36*, 296−313. (c) Davis, J. T. *Angew. Chem., Int. Ed.* **2004**, *43*, 668−698. (d) Wang, Y.; Lin, H.-X.; Chen, L.; Ding, S.-Y.; Lei, Z.-C.; Li, D.-Y.; Cao, X.-Y.; Liang, H.-J.; Jiang, Y.-B.; Tian, Z.-Q. *Chem. Soc. Rev.* **2014**, *43*, 399−411.
(5) (a) Stang, P. J.; Olenyuk, B. *Acc. Chem. Res.* **1997**, *30*, 502−518. (b) Seidel, S. R.; Stang, P. J. *Acc. Chem. Res.* **2002**, *35*, 972−983. (c) Fujita, M.; Tominaga, M.; Hori, A.; Therrien, B. *Acc. Chem. Res.*

DOI: 10.1021/jacs.5b06565
J. Am. Chem. Soc. 2015, 137, 11725−11735

2005, *38*, 369−378. (d) Nitschke, J. R. *Acc. Chem. Res.* **2006**, *40*, 103−112. (e) Pluth, M. D.; Raymond, K. N. *Chem. Soc. Rev.* **2007**, *36*, 161−171. (f) Liu, S.; Han, Y.-F.; Jin, G.-X. *Chem. Soc. Rev.* **2007**, *36*, 1543−1560. (g) Oliveri, C. G.; Ulmann, P. A.; Wiester, M. J.; Mirkin, C. A. *Acc. Chem. Res.* **2008**, *41*, 1618−1629. (h) Clever, A. H.; Shionoya, M. *Coord. Chem. Rev.* **2010**, *254*, 2391−2402. (i) Chakrabarty, R.; Mukherjee, P. S.; Stang, P. J. *Chem. Rev.* **2011**, *111*, 6810−6918. (j) Takezawa, Y.; Shionoya, M. *Acc. Chem. Res.* **2012**, *45*, 2066−2076. (k) Cook, T. R.; Zheng, Y.; Stang, P. J. *Chem. Rev.* **2013**, *113*, 734−777. (l) Castilla, A.; Ramsay, W.; Nitschke, J. R. *Acc. Chem. Res.* **2014**, *47*, 2063−2073. (m) Han, M.; Engelhard, D. M.; Clever, G. H. *Chem. Soc. Rev.* **2014**, *43*, 1848. (n) Han, Y.-F.; Jin, G.-X. *Acc. Chem. Res.* **2014**, *47*, 3571−3579. (o) Yoshizawa, M.; Klosterman, J. K. *Chem. Soc. Rev.* **2014**, *43*, 1885−1898.

(6) (a) Fujita, M.; Yazaki, J.; Ogura, K. *J. Am. Chem. Soc.* **1990**, *112*, 5645−5647. (b) Stang, P. J.; Cao, D. H. *J. Am. Chem. Soc.* **1994**, *116*, 4981−4982. (c) Fujita, M.; Oguro, D.; Miyazawa, M.; Oka, H.; Yamaguchi, K.; Ogura, K. *Nature* **1995**, *378*, 469−471. (d) Olenyuk, B.; Levin, M. D.; Whiteford, J. A.; Shield, J. E.; Stang, P. J. *J. Am. Chem. Soc.* **1999**, *121*, 10434−10435. (e) Olenyuk, B.; Whiteford, J. A.; Fechtenkotter, A.; Stang, P. J. *Nature* **1999**, *398*, 796−799. (f) Lee, S. J.; Lin, W. *J. Am. Chem. Soc.* **2002**, *124*, 4554−4555. (g) Kuehl, C. J.; Kryschenko, Y. K.; Radhakrishnan, U.; Seidel, S. R.; Huang, S. D.; Stang, P. J. *Proc. Natl. Acad. Sci. U. S. A.* **2002**, *99*, 4932−4936. (h) Brown, A. M.; Ovchinnikov, M. V.; Stern, C. L.; Mirkin, C. A. *J. Am. Chem. Soc.* **2004**, *126*, 14316−14137. (i) Nakabayashi, K.; Kawano, M.; Yoshizawa, M.; Ohkoshi, S.; Fujita, M. *J. Am. Chem. Soc.* **2004**, *126*, 16694−16695. (j) Wang, P.; Moorefield, C. N.; Newkome, G. R. *Angew. Chem., Int. Ed.* **2005**, *44*, 1679−1683. (k) Heo, J.; Mirkin, C. A. *Angew. Chem., Int. Ed.* **2006**, *45*, 941−944. (l) Dong, V. M.; Fiedler, D.; Carl, B.; Bergman, R. G.; Raymond, K. N. *J. Am. Chem. Soc.* **2006**, *128*, 14464−14465. (m) Harano, K.; Hiraoka, S.; Shionoya, M. *J. Am. Chem. Soc.* **2007**, *129*, 5300−5301. (n) Bar, A. K.; Chakrabarty, R.; Mostafa, G.; Mukherjee, P. S. *Angew. Chem., Int. Ed.* **2008**, *47*, 8455−8459. (o) Meng, W.; Clegg, J. K.; Thoburn, J. D.; Nitschke, J. R. *J. Am. Chem. Soc.* **2011**, *133*, 13652−13660. (p) Clever, G. H.; Kawamura, W.; Tashiro, S.; Shiro, M.; Shionoya, M. *Angew. Chem., Int. Ed.* **2012**, *51*, 2602−2609. (q) Wang, M.; Wang, C.; Hao, X.-Q.; Li, X.; Vaughn, T. J.; Zhang, Y.-Y.; Yu, Y.; Li, Z.-Y.; Song, M.-P.; Yang, H.-B.; Li, X. *J. Am. Chem. Soc.* **2014**, *136*, 10499−10507. (r) Wood, C. S.; Ronson, T. K.; Belenguer, A. M.; Holstein, J. J.; Nitschke, J. R. *Nat. Chem.* **2015**, *7*, 354−358.

(7) (a) Northrop, B. H.; Yang, H.-B.; Stang, P. J. *Chem. Commun.* **2008**, 5896−5908. (b) Xu, L.; Chen, L.-J.; Yang, H.-B. *Chem. Commun.* **2014**, *50*, 5156−5170. (c) Xu, L.; Wang, Y.-X.; Yang, H.-B. *Dalton Trans.* **2015**, *44*, 867−890. (d) Xu, L.; Wang, Y.-X.; Chen, L.-J.; Yang, H.-B. *Chem. Soc. Rev.* **2015**, *44*, 2148−2167. (e) McConnell, A. J.; Wood, C. S.; Neelakandan, P. P.; Nitschke, J. R. *Chem. Rev.* **2015**, *115*, 7729−7793.

(8) (a) Mukherjee, P. S.; Min, K. S.; Arif, A. M.; Stang, P. J. *Inorg. Chem.* **2004**, *43*, 6345−6350. (b) Yang, H.-B.; Das, N.; Huang, F.; Hawkridge, A. M.; Muddiman, D. C.; Stang, P. J. *J. Am. Chem. Soc.* **2006**, *128*, 10014−10015. (c) Harano, K.; Hiraoka, S.; Shionoya, M. *J. Am. Chem. Soc.* **2007**, *129*, 5300−5301. (d) Yang, H.-B.; Ghosh, K.; Zhao, Y.; Northrop, B. H.; Lyndon, M. M.; Muddiman, D. C.; White, H. S.; Stang, P. J. *J. Am. Chem. Soc.* **2008**, *130*, 839−841. (e) Hiraoka, S.; Harano, K.; Shiro, M.; Shionoya, M. *J. Am. Chem. Soc.* **2008**, *130*, 14368−14369. (f) Ghosh, S.; Gole, B.; Bar, A. K.; Mukherjee, P. S. *Organometallics* **2009**, *28*, 4288−4296. (g) Ghosh, S.; Chakrabarty, R.; Mukherjee, P. S. *Inorg. Chem.* **2009**, *48*, 549−556. (h) Kent, C. A.; Liu, D.; Meyer, T. J.; Lin, W. *J. Am. Chem. Soc.* **2012**, *134*, 3991−3994. (i) Han, M.; Michel, R.; He, B.; Chen, Y.-S.; Stalke, D.; John, M.; Clever, G. H. *Angew. Chem., Int. Ed.* **2013**, *52*, 1319−1323. (j) Freye, S.; Michel, R.; Stalke, D.; Pawliczek, M.; Frauendorf, H.; Clever, G. H. *J. Am. Chem. Soc.* **2013**, *135*, 8476−8479. (k) Kishi, N.; Akita, M.; Kamiya, M.; Hayashi, S.; Hsu, H.-F.; Yoshizawa, M. *J. Am. Chem. Soc.* **2013**, *135*, 12976−12979. (l) He, C.; Lu, K.; Liu, D.; Lin, W. *J. Am. Chem. Soc.* **2014**, *136*, 5181−5184. (m) Roberts, D. A.; Castilla, A. M.; Ronson, T. K.; Nitschke, J. R. *J. Am. Chem. Soc.* **2014**, *136*, 8201−8204. (n) Samanta, D.; Mukherjee, P. S. *J. Am. Chem. Soc.* **2014**, *136*, 17006−17009. (o) Acharyya, K.; Mukherjee, P. S. *Chem. Commun.* **2014**, *50*, 15788−15791. (p) Shanmugaraju, S.; Mukherjee, P. S. *Chem. - Eur. J.* **2015**, *21*, 6656−6666. (q) Zhu, R.; Lübben, J.; Dittrich, B.; Clever, G. H. *Angew. Chem., Int. Ed.* **2015**, *54*, 2796−2800.

(9) (a) Zhao, G.-Z.; Li, Q.-J.; Chen, L.-J.; Tan, H.; Wang, C.-H.; Lehman, D. A.; Muddiman, D. C.; Yang, H.-B. *Organometallics* **2011**, *30*, 3637−3642. (b) Zhao, G.-Z.; Li, Q.-J.; Chen, L.-J.; Tan, H.; Wang, C.-H.; Wang, D.-X.; Yang, H.-B. *Organometallics* **2011**, *30*, 5141−5143. (c) Chen, L.-J.; Li, Q.-J.; He, J.; Tan, H.; Abliz, Z.; Yang, H.-B. *J. Org. Chem.* **2012**, *77*, 1148−1153. (d) Han, Q.; Wang, L.-L.; Li, Q.-J.; Zhao, G.-Z.; He, J.; Hu, B.; Tan, H.; Abliz, Z.; Yu, Y.; Yang, H.-B. *J. Org. Chem.* **2012**, *77*, 3426−3432. (e) Chen, S.; Chen, L.-J.; Yang, H.-B.; Tian, H.; Zhu, W. *J. Am. Chem. Soc.* **2012**, *134*, 13596−13599. (f) Wu, N.-W.; Zhang, J.; Ciren, D.; Han, Q.; Chen, L.-J.; Xu, L.; Yang, H.-B. *Organometallics* **2013**, *32*, 2536−2545. (g) Ou-Yang, J.-K.; Zhang, Y.-Y.; He, M.-L.; Li, J.-T.; Li, X.; Zhao, X.-L.; Wang, C.-H.; Yu, Y.; Wang, D.-X.; Xu, L.; Yang, H.-B. *Org. Lett.* **2014**, *16*, 664−667. (h) Wang, W.; Zhang, Y.; Sun, B.; Chen, L.-J.; Xu, X.-D.; Wang, M.; Li, X.; Yu, Y.; Jiang, W.; Yang, H.-B. *Chem. Sci.* **2014**, *5*, 4554−4560. (i) Wang, W.; Sun, B.; Wang, X.-Q.; Ren, Y.-Y.; Chen, L.-J.; Ma, J.; Zhang, Y.; Li, X.; Yu, Y.; Tan, H.; Yang, H.-B. *Chem. - Eur. J.* **2015**, *21*, 6286−6294.

(10) (a) Zhao, G.-Z.; Chen, L.-J.; Wang, W.; Zhang, J.; Yang, G.; Wang, D.; Yu, Y.; Yang, H.-B. *Chem. - Eur. J.* **2013**, *19*, 10094−10100. (b) Li, Z.-Y.; Xu, L.; Wang, C.-H.; Zhao, X.-L.; Yang, H.-B. *Chem. Commun.* **2013**, *49*, 6194−6196. (c) Li, Z.-Y.; Zhang, Y.-Y.; Zhang, C.-W.; Chen, L.-J.; Wang, C.; Tan, H.; Yu, Y.; Li, X.; Yang, H.-B. *J. Am. Chem. Soc.* **2014**, *136*, 8577−8589. (d) Wu, N.-W.; Chen, L.-J.; Wang, C.; Ren, Y.-Y.; Li, X.; Xu, L.; Yang, H.-B. *Chem. Commun.* **2014**, *50*, 4231−4233. (e) Chen, L.-J.; Zhao, G.-Z.; Jiang, B.; Sun, B.; Wang, M.; Xu, L.; He, J.; Abliz, Z.; Tan, H.; Li, X.; Yang, H.-B. *J. Am. Chem. Soc.* **2014**, *136*, 5993−6001. (f) Zhang, J.; Marega, R.; Chen, L.-J.; Wu, N.-W.; Xu, X.-D.; Muddiman, D. C.; Bonifazi, D.; Yang, H.-B. *Chem. - Asian J.* **2014**, *9*, 2928−2936. (g) Sun, B.; Wang, M.; Lou, Z.; Huang, M.; Xu, C.; Li, X.; Chen, L.-J.; Yu, Y.; Davis, G. L.; Xu, B.; Yang, H.-B.; Li, X. *J. Am. Chem. Soc.* **2015**, *137*, 1556−1564.

(11) (a) Baytekin, H. T.; Sahre, M.; Rang, A.; Engeser, M.; Schulz, A.; Schalley, C. A. *Small* **2008**, *4*, 1823−1834. (b) Chan, Y.; Moorefield, C. N.; Soler, M.; Newkome, G. R. *Chem. - Eur. J.* **2010**, *16*, 1768−1771. (c) Yan, X.; Jiang, B.; Cook, T. R.; Zhang, Y.; Li, J.; Yu, Y.; Huang, F.; Yang, H.-B.; Stang, P. J. *J. Am. Chem. Soc.* **2013**, *135*, 16813−16816. (d) Yan, X.; Li, S.; Cook, T. R.; Ji, X.; Yao, Y.; Pollock, J. B.; Shi, Y.; Yu, G.; Li, J.; Huang, F.; Stang, P. J. *J. Am. Chem. Soc.* **2013**, *135*, 14036−14039. (e) Yan, X.; Li, S.; Pollock, J. B.; Cook, T. R.; Chen, J.; Zhan, Y.; Ji, X.; Yu, Y.; Huang, F.; Stang, P. J. *Proc. Natl. Acad. Sci. U. S. A.* **2013**, *110*, 15585−15590. (f) Yan, X.; Cook, T. R.; Pollock, J. B.; Wei, P.; Zhang, Y.; Yu, Y.; Huang, F.; Stang, P. J. *J. Am. Chem. Soc.* **2014**, *136*, 4460−4463. (g) Wei, P.; Cook, T. R.; Yan, X.; Huang, F.; Stang, P. J. *J. Am. Chem. Soc.* **2014**, *136*, 15497−15500.

(12) (a) Kumar, S.; Nussinov, R. *ChemBioChem* **2002**, *3*, 604−617. (b) Carrivain, P.; Cournac, A.; Lavelle, C.; Lesne, A.; Mozziconacci, J.; Paillusson, F.; Signon, L.; Victor, J.; Barbi, M. *Soft Matter* **2012**, *8*, 9285−9301. (c) Taira, T.; Ajami, D.; Rebek, J., Jr. *J. Am. Chem. Soc.* **2012**, *134*, 11971−11973. (d) Davis, J. T. *Nat. Chem.* **2014**, *6*, 852−853.

(13) (a) Sastry, M.; Rao, M.; Ganesh, K. N. *Acc. Chem. Res.* **2002**, *35*, 847−855. (b) Kostiainen, M. A.; Hiekkataipale, P.; Laiho, A.; Lemieux, V.; Seitsonen, J.; Ruokolainen, J.; Ceci, P. *Nat. Nanotechnol.* **2013**, *8*, 52−56.

(14) Oosta, G. M.; Gardner, W. T.; Beeler, D. L.; Rosenberg, R. D. *Proc. Natl. Acad. Sci. U. S. A.* **1981**, *78*, 829−833.

(15) (a) Capila, I.; Linhardt, R. J. *Angew. Chem.* **2002**, *114*, 426−450; *Angew. Chem., Int. Ed.* **2002**, *41*, 390−412. (b) Mid-deldorp, S. *Thromb. Res.* **2008**, *122*, 753−762.

(16) (a) Zhao, Z.; Lam, J. W. Y.; Tang, B. Z. *J. Mater. Chem.* **2012**, *22*, 23726−23740. (b) Yu, Y.; Qin, A.; Feng, C.; Lu, P.; Ng, K. M.; Luo, K. Q.; Tang, B. Z. *Analyst* **2012**, *137*, 5592−5596. (c) Zhao, E.; Hong, Y.; Chen, S.; Leung, C. W. T.; Chan, C. Y. K.; Kwok, R. T. K.;

DOI: 10.1021/jacs.5b06565
J. Am. Chem. Soc. 2015, 137, 11725−11735

Lam, J. W. Y.; Tang, B. Z. *Adv. Healthcare Mater.* **2014**, *3*, 88−96. (d) Yuan, W. Z.; Tan, Y.; Gong, Y.; Lu, P.; Lam, J. W. Y.; Shen, X. Y.; Feng, C.; Sung, H. H-Y.; Lu, Y.; Williams, I. D.; Sun, J. Z.; Zhang, Y.; Tang, B. Z. *Adv. Mater.* **2013**, *25*, 2837−2843. (e) Yan, X.; Cook, T. R.; Wang, P.; Huang, F.; Stang, P. J. *Nat. Chem.* **2015**, *7*, 342−348.

(17) (a) Mei, J.; Hong, Y.; Lam, J. W. Y.; Qin, A.; Tang, Y.; Tang, B. Z. *Adv. Mater.* **2014**, *26*, 5429−5479. (b) Hong, Y.; Lam, J. W. Y.; Tang, B. Z. *Chem. Soc. Rev.* **2011**, *40*, 5361−5388. (c) Hong, Y.; Lam, J. W. Y.; Tang, B. Z. *Chem. Commun.* **2009**, 4332−4353. (d) Ding, D.; Li, K.; Liu, B.; Tang, B. Z. *Acc. Chem. Res.* **2013**, *46*, 2441−2453.

(18) (a) Luo, J.; Xie, Z.; Lam, J. W. Y.; Cheng, L.; Chen, H.; Qiu, C.; Kwok, H. S.; Zhan, X.; Liu, Y.; Zhu, D.; Tang, B. Z. *Chem. Commun.* **2001**, 1740−1741. (b) Liu, Y.; Deng, C.; Tang, L.; Qin, A.; Hu, R.; Sun, J. Z.; Tang, B. Z. *J. Am. Chem. Soc.* **2011**, *133*, 660−663. (c) Wang, J.; Mei, J.; Hu, R.; Sun, J. Z.; Qin, A.; Tang, B. Z. *J. Am. Chem. Soc.* **2012**, *134*, 9956−9966. (d) Leung, C. W. T.; Hong, Y.; Chen, S.; Zhao, E.; Lam, J. W. Y.; Tang, B. Z. *J. Am. Chem. Soc.* **2013**, *135*, 62−65.

(19) Bromfield, S. M.; Wilde, E.; Smith, D. K. *Chem. Soc. Rev.* **2013**, *42*, 9184−9195.

(20) Hermans, C.; Claeys, D. *Curr. Med. Res. Opin.* **2006**, *22*, 471−481.

(21) Hu, R.; Lager, E.; Aguilar-Aguilar, A.; Liu, J.; Lam, J.; Sung, H.; Williams, I.; Zhong, Y.; Wong, K.; Pena-Cabrera, E.; Tang, B. Z. *J. Phys. Chem. C* **2009**, *113*, 15845−15853.

(22) (a) Pu, K. Y.; Liu, B. *Adv. Funct. Mater.* **2009**, *19*, 277−284. (b) Ling, Y.; Gao, Z. F.; Zhou, Q.; Li, N. B.; Luo, H. Q. *Anal. Chem.* **2015**, *87*, 1575−1581. (c) Bromfield, S. M.; Barnard, A.; Posocco, P.; Fermeglia, M.; Pricl, S.; Smith, D. K. *J. Am. Chem. Soc.* **2013**, *135*, 2911−2914.

(23) (a) Szelke, H.; Schubel, S.; Harenberg, J.; Kramer, R. *Chem. Commun.* **2010**, *46*, 1667−1669. (b) Xu, B.; Wu, X.; Li, H.; Tong, H.; Wang, L. *Polymer* **2012**, *53*, 490−494. (c) Chen, D.; Shi, J.; Wu, Y.; Tong, B.; Zhi, J.; Dong, Y. *Sci. China: Chem.* **2013**, *56*, 1239−1246. (d) Liu, H.; Song, P.; Wei, R.; Li, K.; Tong, A. *Talanta* **2014**, *118*, 348−352.

DOI: 10.1021/jacs.5b06565
J. Am. Chem. Soc. 2015, 137, 11725−11735